Reducing bias and variance for CTF estimation in single particle cryo-EM

黃峻祿

The paper's doi: https://doi.org/10.1016/j.ultramic.2020.112950 and the paper's authors: A. Heimowitz, *et al*.

Group meeting,
ISS, AS
28/09/2021

Content

- Motivation and Problem
- Methods
  - Power spectrum estimation
  - Background subtraction
  - CTF parameter estimation
- Results
- Conclusion

Motivation

- Single particle cryo-EM becomes a leading tool for resolving the 3D structure of macromolecules. Cryo-EM produced a set of micrographs which contain several 2D particle projections. The micrographs are contaminated. The 2D projections are also distorted by convolution with a point spread function, PSF. It is therefore important to estimate PSF and account for it during reconstruction.

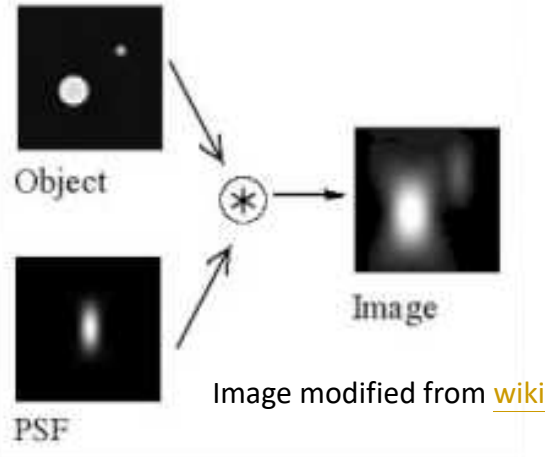

Image modified from wiki

Reminder of CTF and ASPIRE-CTF

- It is convenient to consider the Fourier transform of the PSF which is the contrast transfer function, CTF.
  - The CTF has a simple expression in the polar coordinates of the spatial frequency.
  - The CTF's effect is directly visible in the frequency domain where the CTF acts as a pointwise multiplication rather than a convolution.
- This paper provides ASPIRE-CTF [1] which is a new method for the CTF estimation.

[1]: https://github.com/ComputationalCryoEM/ASPIRE-Python

Pipeline of ASPIRE-CTF

Input: movies

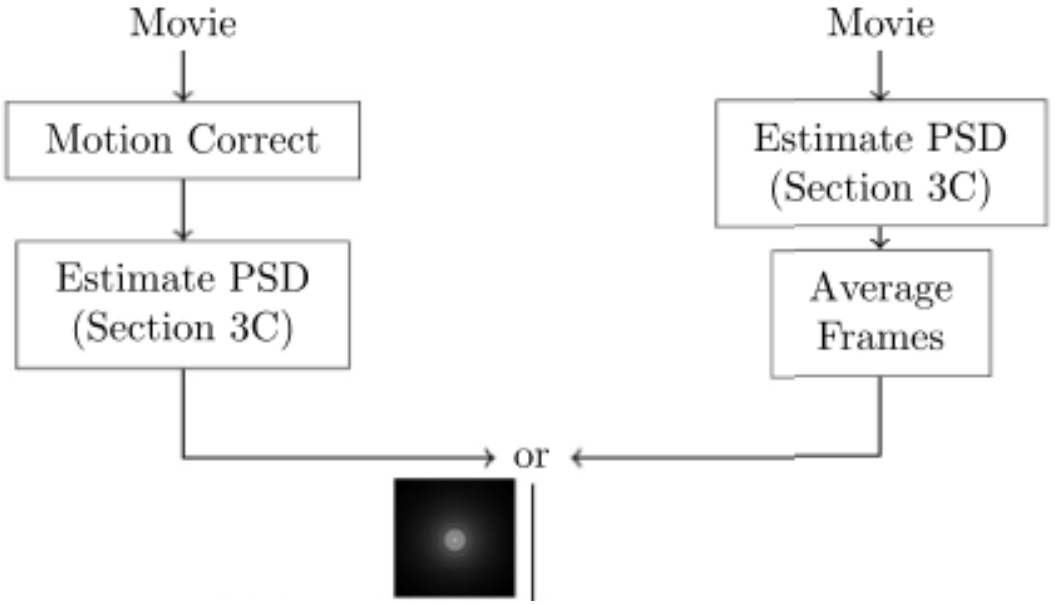

Power spectrum estimations which are then inputs for the right pipeline

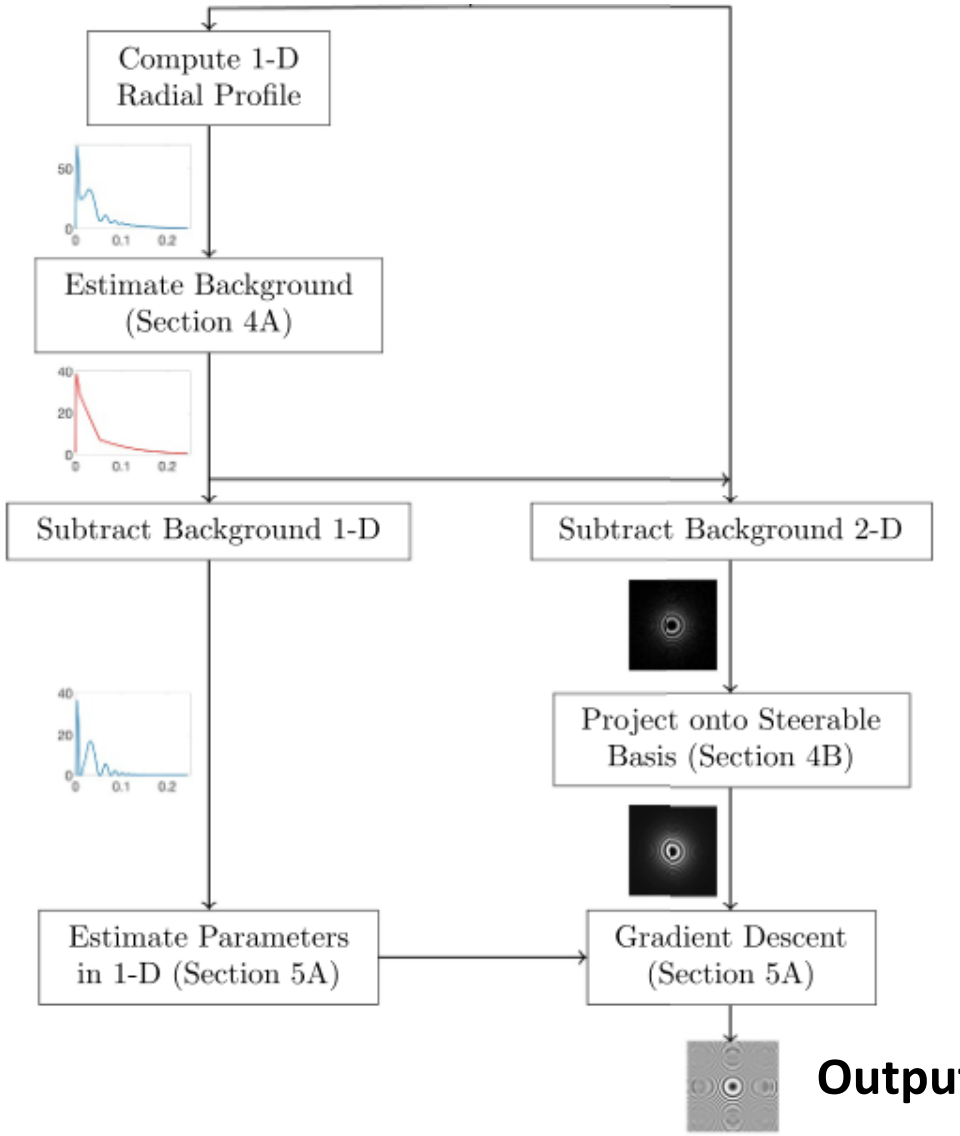

Output: CTF

Cryo-EM image formation and CTF (1)

- In cryo-EM, a micrograph contains 2D projections of each particle. This process is described by linear model:

$$\mathbf{y} = h_\phi * \mathbf{x} + \mathbf{e}$$

Observed micrograph, **y**
Tomographic projection, **x**
Noise, **e**
Point spread function, h_ϕ, depending on a vector ϕ

- The clean, and background-subtracted micrograph is $\mathbf{z} = h_\phi * \mathbf{x}$.

- The Fourier transform of h_ϕ is the CTF [1],

$$H_\phi(\mathbf{g}) = -\sin(\chi_\phi(\mathbf{g}))$$

$\mathbf{g}$ is the spatial frequency
The phase, $\chi_\phi(\mathbf{g})$, is given in backup

- The astigmatic defocus depth:

$$\Delta f_\phi(\alpha) = \Delta f_1 + \Delta f_2 + (\Delta f_1 - \Delta f_2)\cos(2\alpha - 2\alpha_f)$$

Polar angle, α, depending on $\mathbf{g}$;
Major and minor defocus depths, Δf_1, Δf_2;
Defocus angle, α_f

[1]: A. Rohou, N. Grigorieff, CTFFIND4: fast and accurate defocus estimation from electron micrographs, J. Struct. Biol. 192 (2) (2015) 216-221

Cryo-EM image formation and CTF (2)

- The defocus vector, ϕ, can be formed and expressed by $\phi = (\Delta f_1, \Delta f_2, \alpha_f)$ which parametrizes CTF.
  - Δf_1 and Δf_2 determine the amount of defocus along two perpendicular axes;
  - $\Delta f_1 - \Delta f_2$ measures the amount of astigmatism in CTF;
  - α_f specifies the counterclockwise angle between the major defocus axis and the positive x-axis.

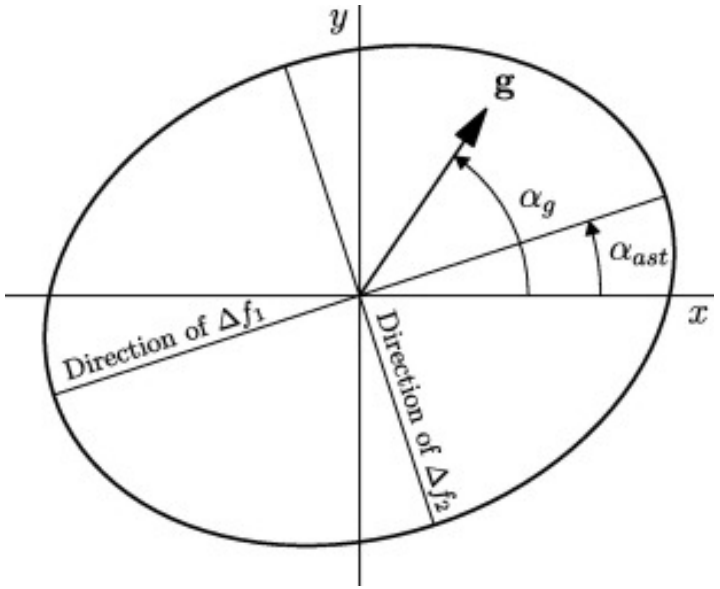

Coordinate for CTF, where $\alpha_{ast} = \alpha_f$ and $\alpha_g = \alpha$.
Figure from [A. Rohou et al., CTFFIND4, (2015)]

Visualization of the effect on astigmatism

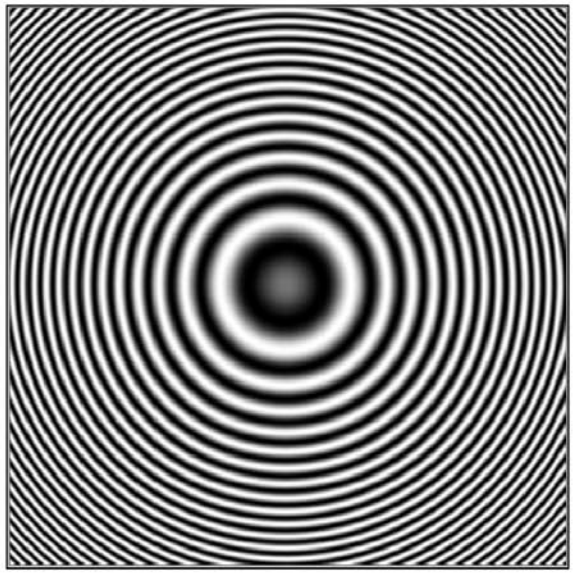

(a)

Radially symmetric CTF, $\frac{\Delta f_1 - \Delta f_2}{\Delta f_1 + \Delta f_2} = 0$

Non-astigmatic case

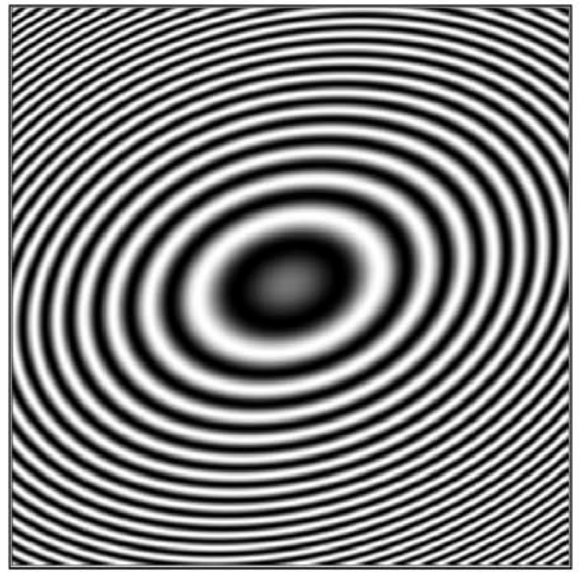

(b)

Highly astigmatic CTF, $\frac{\Delta f_1 - \Delta f_2}{\Delta f_1 + \Delta f_2} = \frac{1}{2}$

Power spectrum

- The power spectra $S_{\mathbf{x}}$, $S_{\mathbf{y}}$ and $S_{\mathbf{e}}$ are related by

$$S_{\mathbf{y}}(\mathbf{g}) = \left|H_{\phi}(\mathbf{g})\right|^2 S_{\mathbf{x}}(\mathbf{g}) + S_{\mathbf{e}}(\mathbf{g})$$

  - $S_{\mathbf{x}}$ and $S_{\mathbf{e}}$ are slowly decaying while $\left|H_{\phi}(\mathbf{g})\right|^2$ oscillates rapidly

    → $S_{\mathbf{y}} - S_{\mathbf{e}}$ is approximately proportional to $\left|H_{\phi}(\mathbf{g})\right|^2$

    → may estimate $S_{\mathbf{y}} - S_{\mathbf{e}}$ and maximize its correlation with $\left|H_{\phi}(\mathbf{g})\right|^2$ in order to estimate ϕ
  - $S_{\mathbf{y}}(\mathbf{g}) - S_{\mathbf{e}}(\mathbf{g}) = 0$ when zero crossing, $H_{\phi}(\mathbf{g}) = 0$, appears.

The experimental power spectrum $S_{\mathbf{y}}$ is the squared magnitudes of Fourier transforming the observed micrograph: $\{\mathrm{FT}[y]\}^2$.

power spectrum estimation—periodogram

- The periodogram estimates a common power spectrum:

$$\hat{S}_{\mathbf{y}}^{(\mathrm{p})} = \frac{1}{N^2}\left|\sum_{k_1,k_2=0}^{N-1} \mathbf{y}[k_1,k_2]\mathrm{e}^{-\mathrm{j}2\pi(\mathrm{g}_1 k_1+\mathrm{g}_2 k_2)}\right|^2,$$

for $\mathbf{g} \in \left[-\frac{1}{2},\frac{1}{2}\right]^2$, given by the values $\mathbf{y}[k_1,k_2]$ for $(k_1,k_2) \in \{0,1,\dots,N-1\}^2$ with an $N \times N$ sample of $\mathbf{y}$.

  - $\hat{S}_{\mathbf{y}}^{(\mathrm{p})}(\mathbf{g})$ is typically calculated on $N \times N$ grid, $M_N = \left\{-\frac{1}{2},-\frac{1}{2}+\frac{2}{N},\dots,\frac{1}{2}-\frac{2}{N}\right\}^2$

- This enables the use of fast Fourier transforms, FFTs, for computing the periodogram with $O(N^2 \log N)$ → the peirodgram is a popular estimator in cryo-EM.

Mean square error

- In order to see how the periodogram well-estimates a power spectrum,

the mean square error, MSE, of $\hat{S}_{\mathbf{y}}^{(\mathrm{p})}$ at $\mathbf{g}$ is used and is given by

$$\mathrm{MSE}\left(\hat{S}_{\mathbf{y}}^{(\mathrm{p})}(\mathbf{g})\right) = \mathbb{E}\left[\left|\hat{S}_{\mathbf{y}}^{(\mathrm{p})}(\mathbf{g}) - S_{\mathrm{y}}(\mathbf{g})\right|^2\right],$$

- The MSE has two sources, bias and variance.

$$\mathrm{MSE}\left(\hat{S}_{\mathbf{y}}^{(\mathrm{p})}(\mathbf{g})\right) = \mathrm{Bias}^2\left(\hat{S}_{\mathbf{y}}^{(\mathrm{p})}(\mathbf{g})\right) + \mathrm{Var}\left(\hat{S}_{\mathbf{y}}^{(\mathrm{p})}(\mathbf{g})\right)$$

Bias measures the deviation of the expectation from the true value, while variance measures the average deviation of the periodogram from its expectation.

A low MSE requires low bias and low variance.

Bartlett's method—reducing variance

- With this method, the periodogram estimate is computed for several non-overlapping regions of an image. The estimates are averaged to reduce the variance by a factor approximately equal to the number of regions used.
- Increasing the number of regions by reducing the size of the regions is considered, but, this will increase the bias.
- The authors divide image into *B* non-overlapping blocks, $\mathbf{y}_0, \ldots, \mathbf{y}_{B-1}$ of size $K \times K$. The averaged periodogram is

$$\hat{S}_{\mathbf{y}}^{(\mathrm{b})}(\mathbf{g}) = \frac{1}{B}\sum_{b=0}^{B-1} \hat{S}_{\mathbf{y}_b}^{(\mathrm{p})}(\mathbf{g})$$

Because the block size is $K \times K$ now , sample $\mathbf{g}$ on M_K.

Welch's method—reducing bias

- The expected value of the periodogram estimator is a convolution between the true power spectrum and a 2D Fejér kernel. The Fejér kernel can lead to a high bias.
- Tapering is one of methods to lower the bias of the periodogram estimation. This multiplies the data, **y**, by a taper, **w,** before computing the periodogram. A modified periodogram is then generated.
- The expected value of the modified periodogram is then a convolution between the true power spectrum and a kernel with smaller sidelobes. This reduces the bias of the estimator.
- The taper can be applied to each block produced in Bartlett's method. This is Welch's method which yields the modified periodogram:

$$\hat{S}_{\mathbf{y}}^{(\mathrm{w})}(\mathbf{g}) = \frac{1}{B}\sum_{b=1}^{B} \hat{S}_{\mathbf{y}_b \cdot \mathbf{w}}^{(\mathrm{p})}(\mathbf{g})$$

Multitaper estimators

- Multiple tapers are applied to the blocks, which then yields different estimates of power spectra. The various estimates are averaged to reduces the variance. Higher-order DPSSs* were suited to balance the bias and the variance.

*: discrete prolate spheroidal sequence (DPSS) [D. Slepian, 1978]

$$\hat{S}_{\mathbf{y}}^{(\mathrm{mt})}(\mathbf{g}) = \frac{1}{LB} \sum_{b=0}^{B-1} \sum_{l=0}^{L-1} \hat{S}_{\mathbf{y}_b \cdot \mathbf{w}_l}^{(\mathrm{p})}(\mathbf{g})$$

Example for schematic of multitaper spectral estimation [Prerau *et al*. 2017]

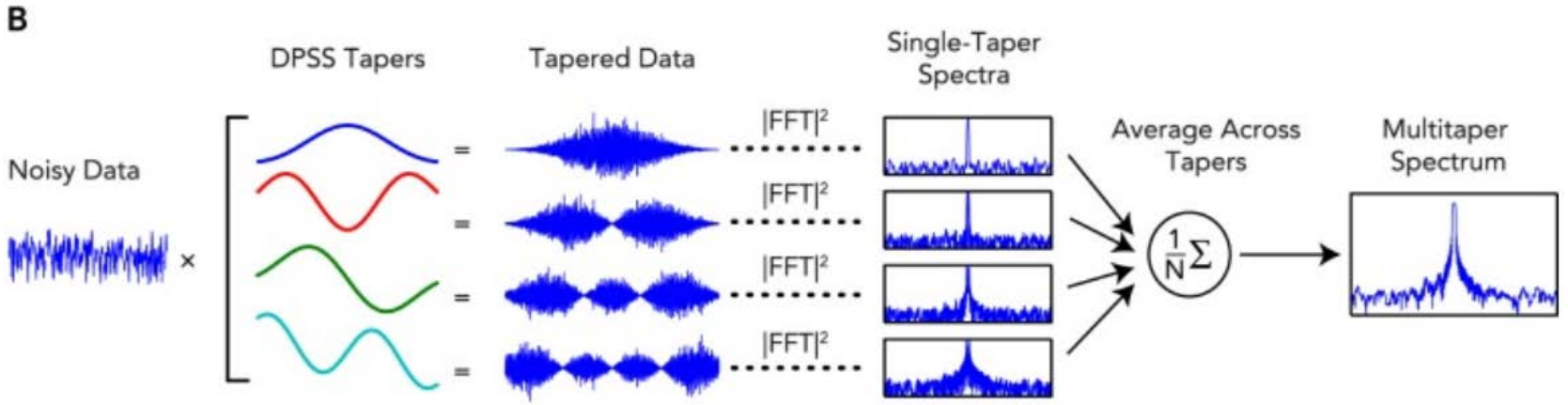

Power spectrum estimation and zero-crossings of the estimation (1)

A β-galactosidase micrograph from the EMPIAR-10017 dataset

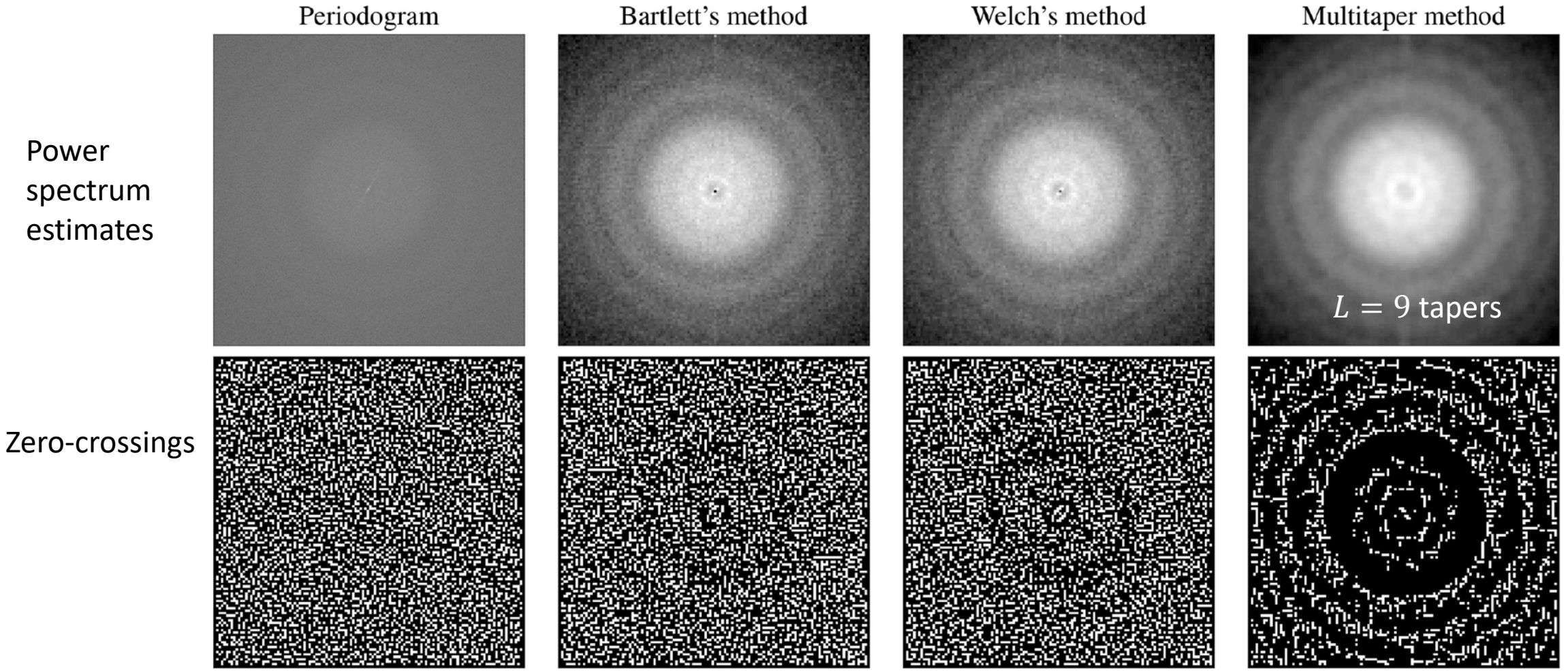

Blocks of size 512×512 were used

Power spectrum estimation and zero-crossings of the estimation (2)

A 80S ribosome micrograph from the EMPIAR-10028 dataset

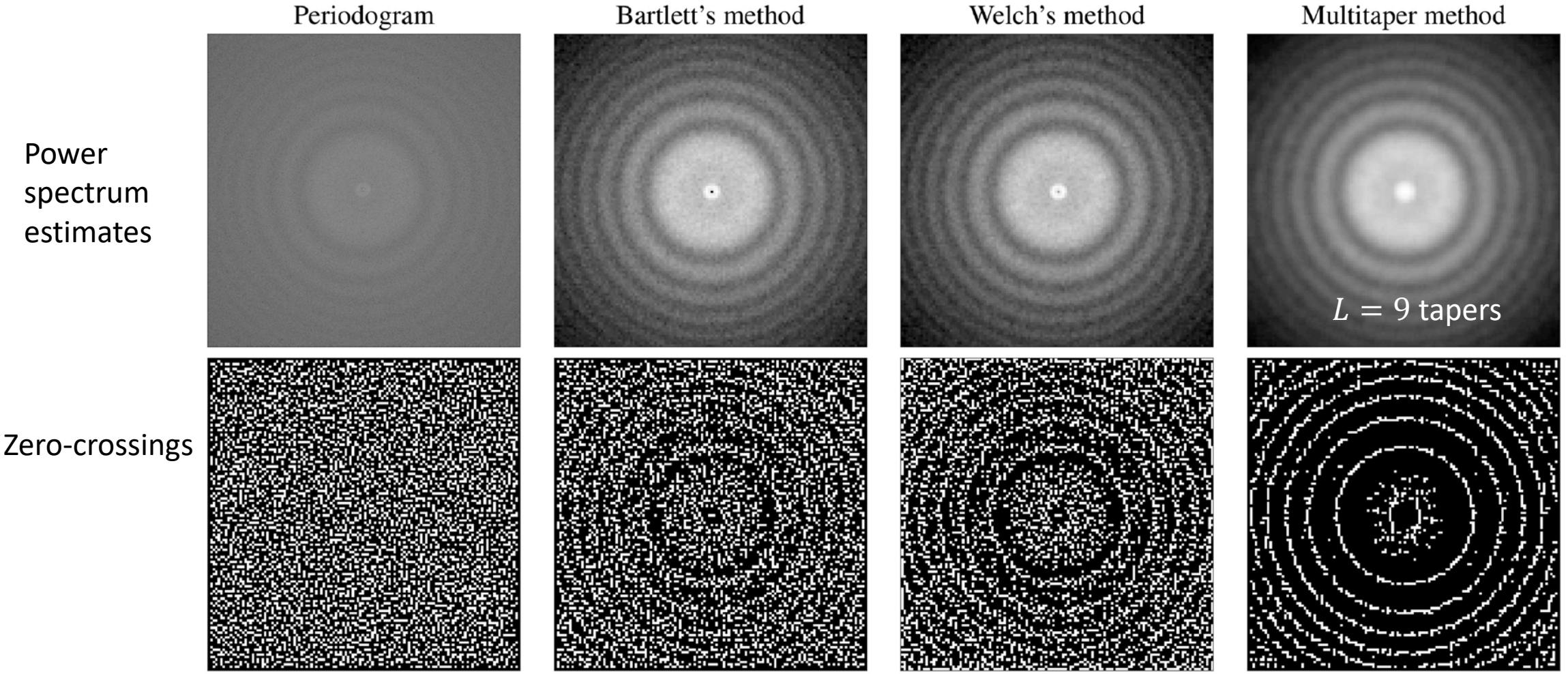

Blocks of size 512×512 were used

Background estimation (1)

- The background-subtracted power spectrum can be expressed as

$$S_{\mathrm{y}}(\mathbf{g}) - S_{\mathbf{e}}(\mathbf{g}) = \left|H_{\phi}(\mathbf{g})\right|^{2} S_{\mathrm{x}}(\mathbf{g})$$

- Background is considered as a radially symmetric and a slowly varying function.
- The background estimation can be obtained by fitting.
  - $S_{\mathbf{e}}(\mathbf{g})$ should coincide with $S_{\mathrm{y}}(\mathbf{g})$ at zero-crossings $H_{\phi}(\mathbf{g})$.
  - $S_{\mathbf{e}}(\mathbf{g})$ should be smaller than or equal to $S_{\mathrm{y}}(\mathbf{g})$ over all spatial frequencies.
  - To estimate $S_{\mathbf{e}}(\mathbf{g})$ is by minimizing $\hat{S}_{\mathbf{y}}^{(\mathrm{mt})} - S_{\mathbf{e}}(\mathbf{g})$.
- In the paper, background is modeled as a non-negative, convex function closest to but no larger than $\hat{S}_{\mathbf{y}}^{(\mathrm{mt})}$, and estimation of the background, S_{e}, is through linear programming.

Background estimation (2)

- The resulting linear program is then

$$\underset{\hat{S}_{\mathbf{e}}}{\text{minimize}} \sum_{r=0,\frac{1}{K},\ldots,\frac{m}{K}} \hat{S}_{\mathbf{y}}^{(\mathrm{mt})}(r) - \hat{S}_{\mathbf{e}}(r)$$

$$\text{subject to } \hat{S}_{\mathbf{e}}(r) \le \hat{S}_{\mathbf{y}}^{(\mathrm{mt})}(r), \qquad r = 0, \ldots, \frac{m}{K}$$

$$\hat{S}_{\mathbf{e}}(r+1) + \hat{S}_{\mathbf{e}}(r-1) \ge \mathbf{2}\hat{S}_{\mathbf{e}}(r), r = 1, \ldots, \frac{m}{K}$$

$$\hat{S}_{\mathbf{e}}(r) \ge 0, r = 0, .., \frac{m}{K}$$

where $\hat{S}_{\mathbf{e}} = [\hat{S}(0), \ldots, \hat{S}(m/K)]^{\boldsymbol{T}}$, and $0 < \frac{m}{K} \le 0.5$ is the spatial frequency above which $\hat{S}_{\mathbf{y}}^{(\mathrm{mt})}(r)$ is dominated by noise. ASPIRE-CTF sets m/K=3/8.

Background estimation (3)

Background estimation for a *β*-galactosidase micrograph from the EMPIAR-10017 dataset

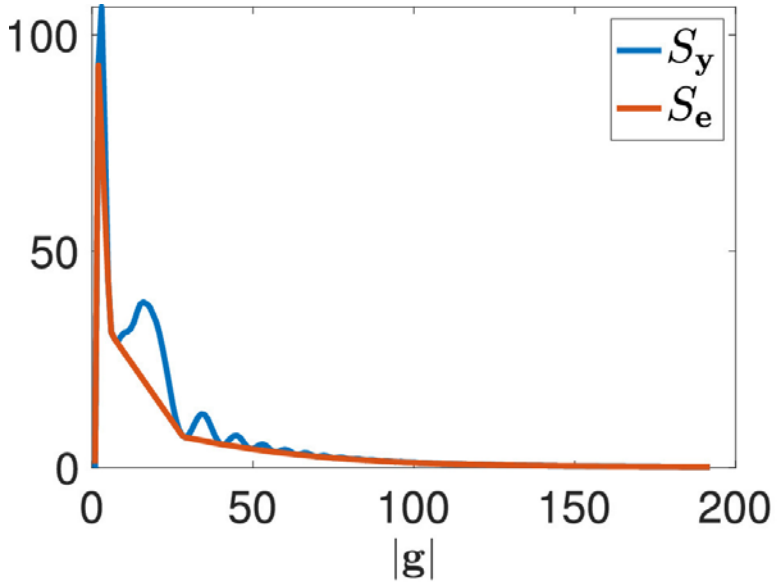

(a)

The 1D radial profile of multi-taper power spectrum estimate, $\hat{S}_{\mathbf{y}}^{(\mathrm{mt})}(r)$, and the estimated background $\hat{S}_{\mathbf{e}}^{(\mathrm{lp})}(r)$

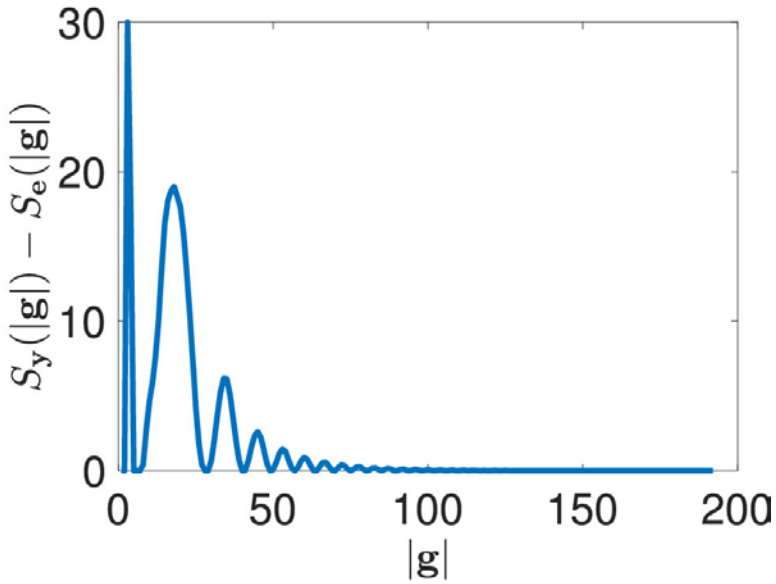

(b)

The background-subtracted 1D radial profile of power spectrum

The background-subtracted power spectrum, $\hat{S}_{\mathbf{y}}^{(\mathrm{mt})}(\mathbf{g}) - \hat{S}_{\boldsymbol{e}}^{(\mathrm{lp})}(\mathbf{g})$, is denoted by $\hat{S}_{\mathbf{z}}^{(\mathrm{lp})}(\mathbf{g})$.

Expansion over a basis (1)

- Reduce the variability of the power spectrum estimator by projecting $\hat{S}_{\mathbf{z}}^{(\mathrm{lp})}(\mathbf{g})$ onto the subspace.
- The subspace can be spanned by a set of steerable basis functions, such as prolate spheroidal wave functions (PSWFs).
- A steerable basis consists of $f_{k,q}(r)e^{\mathrm{j}k\alpha}$, where $k \in \mathbb{Z}$ and $\mathrm{q} = 0, \ldots, p_k - 1$ for some $p_k \geq 0$.
- A given function in polar coordinates can be decomposed in the basis as

$$x(r,\alpha) = \sum_{k=-\infty}^{\infty} \sum_{q=0}^{\infty} a_{k,q} f_{k,q}(r)\, e^{\mathrm{j}k\alpha} \qquad (1)$$

Expansion over a basis (2)

- To determine the steerable basis expansion of CTF, its Taylor expansion around $\Delta f_1 - \Delta f_2 = 0$ is considered.

$$H_\phi(\mathbf{g}) = \sum_{n=0,2,4\ldots}^{P} \frac{(-1)^{\frac{n}{2}+1}}{n!} \sin\left(\chi_\phi^0(r)\right) C_{n,\phi}(\mathbf{g}) + \sum_{n=1,3,5,\ldots}^{P} \frac{(-1)^{\frac{n+1}{2}}}{n!} \cos\left(\chi_\phi^0(r)\right) C_{n,\phi}(\mathbf{g}) + R_P(\mathbf{g}),$$

where $R_P(\mathbf{g})$ is the remainder term.

$R_P(\mathbf{g})$: the remainder term;

$C_{n,\phi}(\mathbf{g}) = \left\{\frac{1}{2}\pi\lambda(\Delta f_1 - \Delta f_2)\cos(2(\alpha - \alpha_f))\frac{r^2}{p^2}\right\}^n$;

$\chi_\phi^0(r) = \frac{1}{2}\pi\lambda r^2(\Delta f_1 + \Delta f_2) - \frac{1}{2}\pi\lambda^3 r^4 C_s + w$ is the non-astigmatic phase function

- The remainder term is bounded by a function of $\left(\frac{\Delta f_1 - \Delta f_2}{\Delta f_1 + \Delta f_2}\right)^{P+1}$ and it is small when astigmatism is small, which is the case for experimental cryo-EM data.

$H_\phi(\mathbf{g}) \approx -\sin\left(\chi_\phi^0(r)\right) - \cos(\chi_\phi^0(r))\, C_{1,\phi}(\mathbf{g})$ is a good approximation of the CTF.

Expansion over a basis (3)

- Because of $\cos\alpha = \frac{1}{2}(e^{\mathrm{j}\alpha} + e^{-\mathrm{j}\alpha})$, the approximated CTF can be expressed:

$$H_\phi(\mathbf{g}) \approx -\sin\left(\chi_\phi^0(r)\right) - \frac{1}{4p^2}\cos\left(\chi_\phi^0(r)\right)\pi\lambda(\Delta f_1 - \Delta f_2)e^{-\mathrm{j}2\alpha_f}r^2e^{\mathrm{j}2\alpha} - \frac{1}{4p^2}\cos\left(\chi_\phi^0(r)\right)\pi\lambda(\Delta f_1 - \Delta f_2)e^{\mathrm{j}2\alpha_f}r^2e^{-\mathrm{j}2\alpha}$$

r and α are the polar coordinates of $\mathbf{g}$

The above formula corresponds to $k = -2,0,2$ cases in Eq. (1).

- The coefficients are computed through an inner product on a $K \times K$ grid:

$$a_{k,q} = \frac{1}{K^2}\sum_{\mathbf{g}\in M_K}\sqrt{\hat{S}_z^{(\mathrm{lp})}(\mathbf{g})}f_{k,q}(r)e^{\mathrm{j}k\alpha}$$

To evaluate Eq. (1) for $a_{k,q}$ and to square the result gives a new power spectrum estimate, $\hat{S}_Z$.

Power spectral density estimates

The results after applying the paper's method on a micrograph from the EMPIAR-10028.

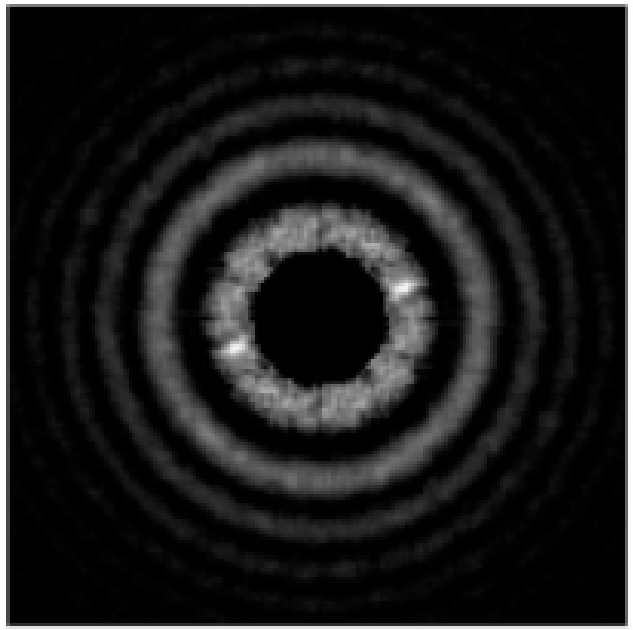

(a)

Background-subtracted estimate $\hat{S}_z^{(lp)}$

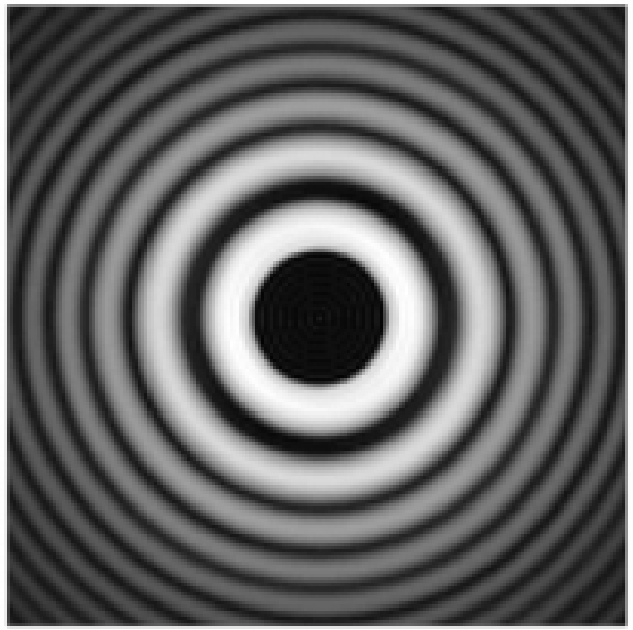

(b)

Projection onto steerable basis function for $k = 0, \pm 2$

The results are smooth enough that many of the zero-crossings of the power spectrum can be easily resolved.

CTF estimation through correlation (1)

- The oscillations in $\left|H_\phi(\mathbf{g})\right|^2 S_\mathbf{x}(\mathbf{g})$ mainly comes from $\left|H_\phi(\mathbf{g})\right|^2$, and $S_\mathbf{x}$ is a slowly-varying function of the radial frequency. Therefore, $\left|H_\phi(\mathbf{g})\right| S_\mathbf{x}^{\frac{1}{2}}(\mathbf{g})$ is proportional to the $\left|H_\phi(\mathbf{g})\right|$.
- Correlation test is a useful tool in estimating CTF parameters. The Pearson correlation of $\left|H_\phi(\mathbf{g})\right|$ and $\hat{S}_z^{1/2}(\mathbf{g})$ is

$$P_{cc}(\phi) = \frac{\sum_{\mathbf{g}\in \mathrm{R}} \left|H_\phi(\mathbf{g})\right| \hat{S}_z^{1/2}(\mathbf{g})}{\left[\sum_{\mathbf{g}\in \mathrm{R}} \left|H_\phi(\mathbf{g})\right|^2 \sum_{\mathbf{g}\in \mathrm{R}} \hat{S}_z(\mathbf{g})\right]^{1/2}}$$

- In order to optimize $P_{cc}(\phi)$, an initial guess for ϕ is needed.
  - Non-astigmatic CTFs, where $\Delta f_1 = \Delta f_2$ [1], and then $\phi = (\Delta f, \Delta f, \alpha_f = 0)$ are considered.
  - R is the set of frequencies over which correlation is computed as $R = \left\{m_1, m_1 + \frac{2}{N}, \ldots, \frac{3}{8}\right\} \times \{0\}$ where m_1 is the first maximum of radial profile of $\hat{S}_\mathrm{z}^{(\mathrm{lp})}(\mathbf{g})$
  - Very low and high frequencies are ignored.
- The Δf which maximizes $P_{cc}(\phi)$ is denoted $\Delta f_\star$.

[1]: K. Zhang, Gctf: real-time CTF determination and correction (2016)

CTF estimation through correlation (2)

- In order to estimate of astigmatism of CTF, the principal directions of the second-order moments of $\hat{S}_z^{1/2}$ is computed. The 2×2 matrix, $\mathbf{M}$, given by

$$M_{1,1} = \sum_{\mathbf{g} \in M_K} \mathrm{g}_1{}^2 \, \hat{S}_{\mathbf{z}}^{\frac{1}{2}}(\mathbf{g}),$$

$$M_{1,2} = M_{2,1} = \sum_{\mathbf{g} \in M_K} \mathrm{g}_1 \mathrm{g}_2 \, \hat{S}_{\mathbf{z}}^{\frac{1}{2}}(\mathbf{g}),$$

$$M_{2,2} = \sum_{\mathbf{g} \in M_K} \mathrm{g}_2{}^2 \, \hat{S}_{\mathbf{z}}^{\frac{1}{2}}(\mathbf{g}).$$

- The eigenvalues, μ_1 and μ_2, of $\mathbf{M}$ estimate the size of major and minor axes in $\hat{S}_z^{1/2}$. Therefore, $\frac{\mu_1}{\mu_2} \cong \frac{\Delta f_1}{\Delta f_2}$ is expected. With the estimated mean defocus $\Delta f_\star = \frac{1}{2}(\Delta f_1 + \Delta f_2)$, we can have

$$\Delta f_{1,\star} = \frac{2\mu_1}{\mu_1 + \mu_2} \Delta f_\star, \; \Delta f_{2,\star} = \frac{2\mu_2}{\mu_1 + \mu_2} \Delta f_\star$$

- The gradient descent on $P_{cc}(\phi)$ is performed to improve the estimation of the defocus parameters.

CTF estimation through correlation (3)

- The image is no longer approximated as non-astigmatic, a set of frequencies over which correlation is computed as $R = M_K$.
- Then the gradient descent at $\phi = (\Delta f_{1,\star}, \Delta f_{2,\star}, \alpha_f)$ is initialized and α_f is set, according to [1], to an arbitrary number, a, for $0 \leq a < \pi/6$ and $(a + \pi/6)$, $(a - \pi/6)$, $(a + \pi/3)$, $(a - \pi/3)$ or $(a - \pi/2)$.
- A run of gradient descent is performed for each α_f.
- The result with the highest value of $P_{cc}(\phi)$ is kept, and its ϕ is the defocus estimate for the micrograph.

[1]: K. Zhang, Gctf: real-time CTF determination and correction (2016)

CTF estimation through zero-crossings

- The background subtracted power spectrum, $\left|H_{\phi}(\mathbf{g})\right|^{2} S_{\mathrm{x}}(\mathbf{g})$, reaches zero at any frequency, the CTF must reach a zero-crossing. Note that $S_{\mathrm{x}}(\mathbf{g})$ is assumed* slowly-varying.
- Any pixel with a value smaller than that of 6-8 neighbor pixels is defined as a zero crossings. Once minima of $\hat{S}_{\mathbf{z}}$ are found, any frequency that is not on a closed ring is discarded.
- Since $H_{\phi}(\mathbf{g}) = -\sin(\chi_{\phi}(\mathbf{g}))$, a zero-crossing appears when $\chi_{\phi}(\mathbf{g}) = \pi l$.

Power spectral density estimates

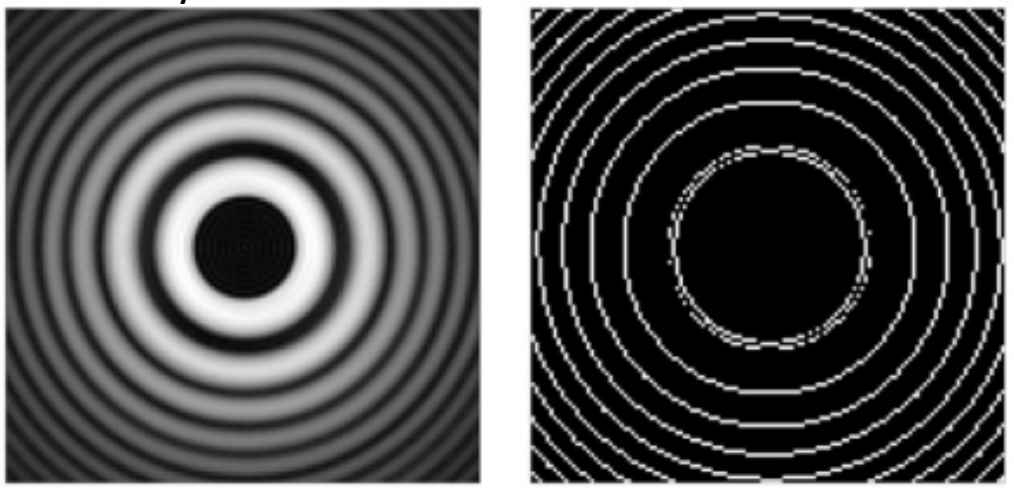

(b) (c)

Projection onto steerable basis function for $k = 0, \pm 2$

Zero crossings of panel (b)

*: even if without the assumption, the fact is that the zero-crossings are known to to create concentric, nearly elliptical rings, centered around the origin.

ASPIRE-CTF application

- The table below shows the datasets are used to estimate CTF by using ASPIRE-CTF.

Dataset	Molecule	Pixel size (Å)	Spherical aberration	Voltage (kV)	Microscope	Detector
EMPIAR-10002	80S ribosome	1.77	2.0	300	Polara	Falcon I
EMPIAR-10028	80S ribosome	1.34	2.0	300	Polara	Falcon II
EMPIAR-10242	2N3R tau filaments	1.04	2.7	300	Titan Krios	Gatan K2 Summit
EMPIAR-10249	HLA dehydrogenase	0.56	2.7	200	Talos Arctica	Gatan K2 Summit

- EMPIAR-10028 and EMPIAR-10242 datasets contain movies and motion-corrected micrographs.
- EMPIAR-10002 and EMPIAR-10249 datasets contain movies only → MotionCor2 is used to produce the motion-corrected micrographs.
- Unless different conditions specified, all experimental results are produced with $L = 4$ tapers and the power spectrum is projected onto the PSWF basis.

Defocus estimation

Three estimated quantity comparisons between using the average power spectrum of the movie frames and using the power spectrum of the motion-corrected micrograph

Average defocus, $\frac{1}{2}(\Delta f_1 + \Delta f_2)$ in nm

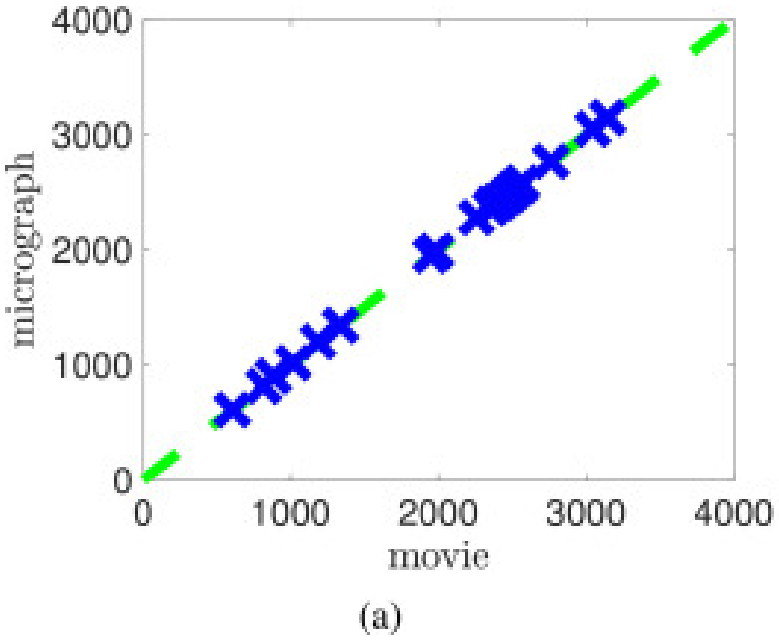

(a)

Astigmatism, $(\Delta f_1 - \Delta f_2)$, in nm

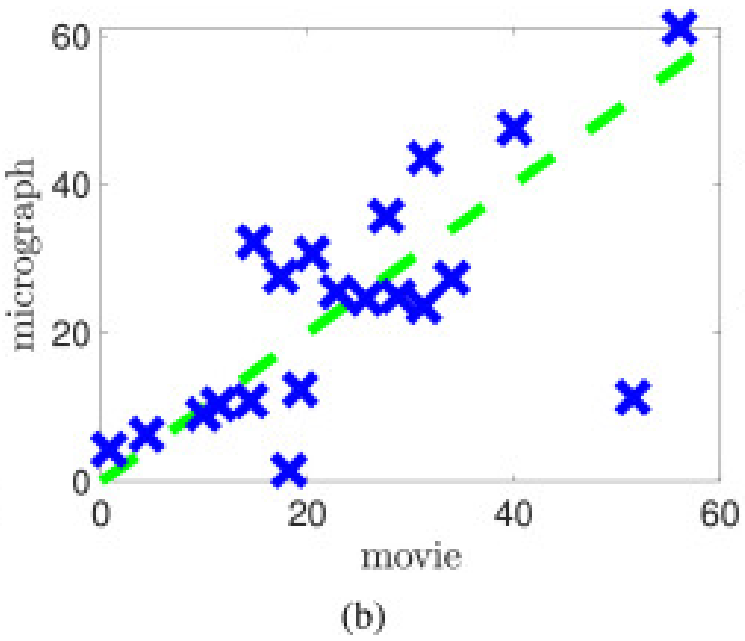

(b)

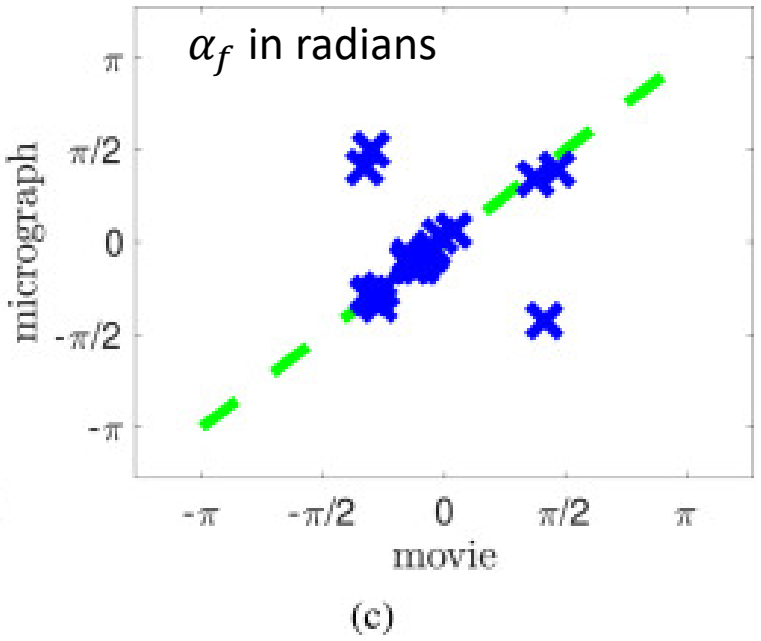

(c)

The estimated quantities from each of the methods are nearly identical.

CTF estimation with CTF challenge

- The CTF challenge consists of almost 200 micrographs which are difficult to determine its CTF.
- The micrographs are divided into half-overlapping blocks of size 512×512 and use $L = 4$ tapers.
  - Background is estimated.
  - Background-subtracted power spectrum is expanded over PSWF basis.
  - The correlation-based method is used to estimate defocus parameters, $\phi_a^{(512)}$.
- For some cases, 512×512 is not sufficient to capture the oscillations of power spectrum.
  - Another half-overlapping blocks of size 1024×1024 is used.
  - The $L = 16$ tapers are then considered.
  - The resulting defocus parameters are denoted by $\phi_a^{(1024)}$.
- The estimated defocus parameters that lead to highest correlation is selected for each method.

$$\phi_j^* = \arg \max_{\phi_j \in \left\{\phi_j^{(512)}, \phi_j^{(1024)}\right\}} \left(\frac{1}{s_t} \sum_{m=1}^{s_t} P_{cc}^m(\phi_j) \right)$$

a: ASPIRE-CTF
g: Gctf
c: CTFFIND4

s_t is the number of micrographs in the t-th dataset, m-th micrographs, and $j \in \{\mathrm{a}, \mathrm{c}, \mathrm{g}\}$

Comparison between quantities estimated by the three methods

Table 2
Comparison between parameters estimated by ASPIRE-CTF, CTFFIND4 and Gctf. We present the mean (over each dataset) of normalized differences between each two CTF estimation methods as detailed in (31). The subscripts *a*, *g* and *c* indicate ASPIRE-CTF, Gctf and CTFFIND4, respectively.

Dataset	Molecule	$\epsilon_{a,g}(\Delta f_1)$	$\epsilon_{a,c}(\Delta f_1)$	$\epsilon_{c,g}(\Delta f_1)$	$\epsilon_{a,g}(\Delta f_2)$	$\epsilon_{a,c}(\Delta f_2)$	$\epsilon_{c,g}(\Delta f_2)$	$\epsilon_{a,g}(\alpha_f)$	$\epsilon_{a,c}(\alpha_f)$	$\epsilon_{c,g}(\alpha_f)$
001	GroEL	0.0157	0.2370	0.2364	0.0155	0.1282	0.6081	1.6599	2.1429	1.3848
002	GroEL	1.3236	1.6500	0.1515	1.4876	0.9746	0.2374	3.6137	5.3979	1.9592
003	60S ribosome	0.0029	0.0049	0.0029	0.0030	0.0032	0.0017	6.1042	6.6618	2.9159
004	60S ribosome	0.0051	0.0130	0.0098	0.0057	0.0406	0.2990	4.2653	2.3667	2.6050
005	apoferritin	0.0036	0.1744	0.8809	0.0036	0.1997	1.5230	0.6597	0.8927	0.7413
006	apoferritin	0.0099	0.2094	0.6392	0.0069	0.3409	1.5217	0.2670	1.3014	1.6142
007	TMV virus	0.0224	0.2144	0.5163	0.0265	0.2674	1.1320	0.4254	0.9891	0.8985
008	TMV virus	0.1961	0.6043	0.3988	0.2163	0.3016	0.5707	3.0253	1.8514	2.8394

For each micrograph, a relative difference between two results obtained from two method is computed. For example,

$$\epsilon_{j,k}(\Delta f_n) = \left[\phi_j(n) - \phi_k(n)\right]/\phi_j(n)$$
$$\epsilon_{j,k}(\alpha_f) = \left[\phi_j(3) - \phi_k(3)\right]/\phi_j(3)$$

where j and k are two different methods such as ASPIRE-CTF, Gctf and CTFFIND4. n is equal to 1 or 2.

$\epsilon_{\mathrm{a,g}}$ or $\epsilon_{\mathrm{a,c}}$ is often smaller than $\epsilon_{\mathrm{g,c}}$

Power spectrum comparison

- The right figure shows a comparison between power spectra obtained by using ASPIRE-CTF, Gctf and CTFFIND4.
- The oscillations of the ASPIRE-CTF power spectra are highly noticeable, which is not the case for the Gctf and CTFFIND4 power spectra.

A sample micrograph of dataset 008 is used.

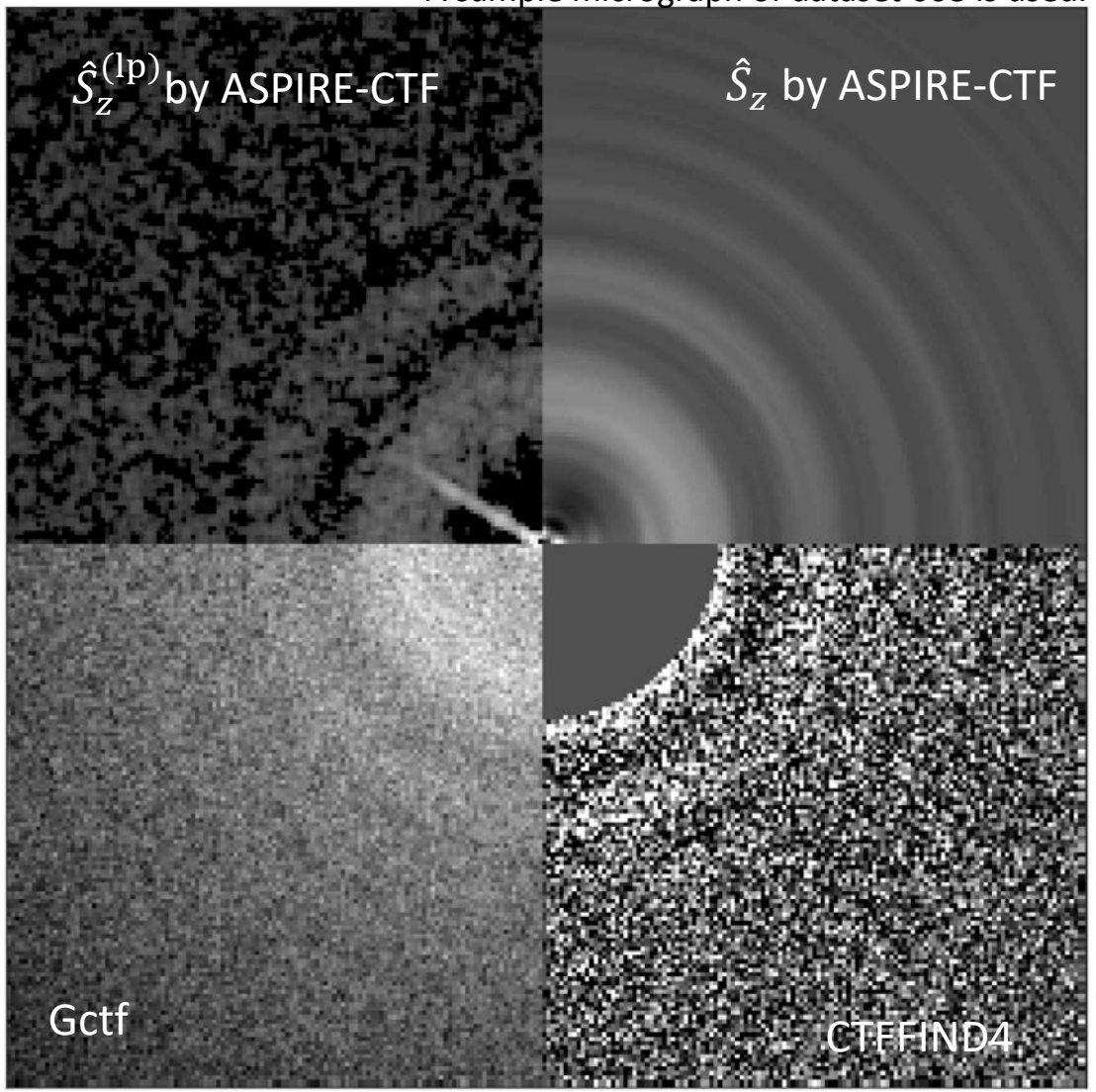

Equipment and runtime

- A 2.6 GHz Intel Core i7 CPU with four cores
- 16 GB of memory

- Runtime for ASPIRE-CTF is 22.5 s on average per micrograph.
- Run time for CTFFIND4 is 541 s.
- Gctf must be run on a GPU so no comparison.

Consistency in low SNR

- In order to test consistency of results with changing SNR, the EMPIAR-10249 dataset is used.
- The dataset contains movies with 44 frames per movie.
- The first frame is disregarded and MotionCor2 is used to create 9 motion-corrected micrographs which summing over motion-corrected frames of 5, 8, 13, 18, 23, 28, 33, 38 and 43.
- The CTF parameters are estimated independently from each micrograph.

Astigmatism as a function of mean defocus for each method. The circles presents the estimations from a micrograph with 43 summed frames.

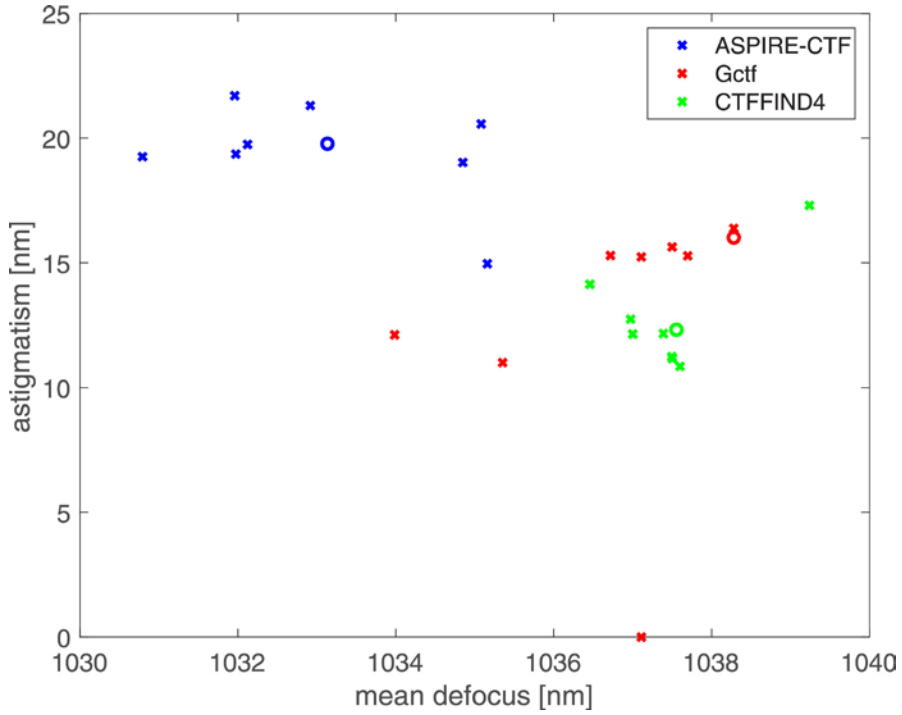

ASPIRE-CTF and CTFFIND4 achieve similar estimates regardless of the number of frames averaged.
Gctf appears a larger error in the astigmatism when 23 frames are used.

Conclusion

- A novel approach for power spectrum estimation of cryo-EM experimental data is presented.
  - Multitaper estimator often leads to reduced MSE, comparing to Bartlett's and Welch's methods.
  - A method for error reduction that is driven directly by the mathematical model of CTF.
- Experiment results on twelve datasets are shown→ their method is suitable for both motion-corrected micrographs and raw movie data.

Backup

Diagram illustrating the formation of images

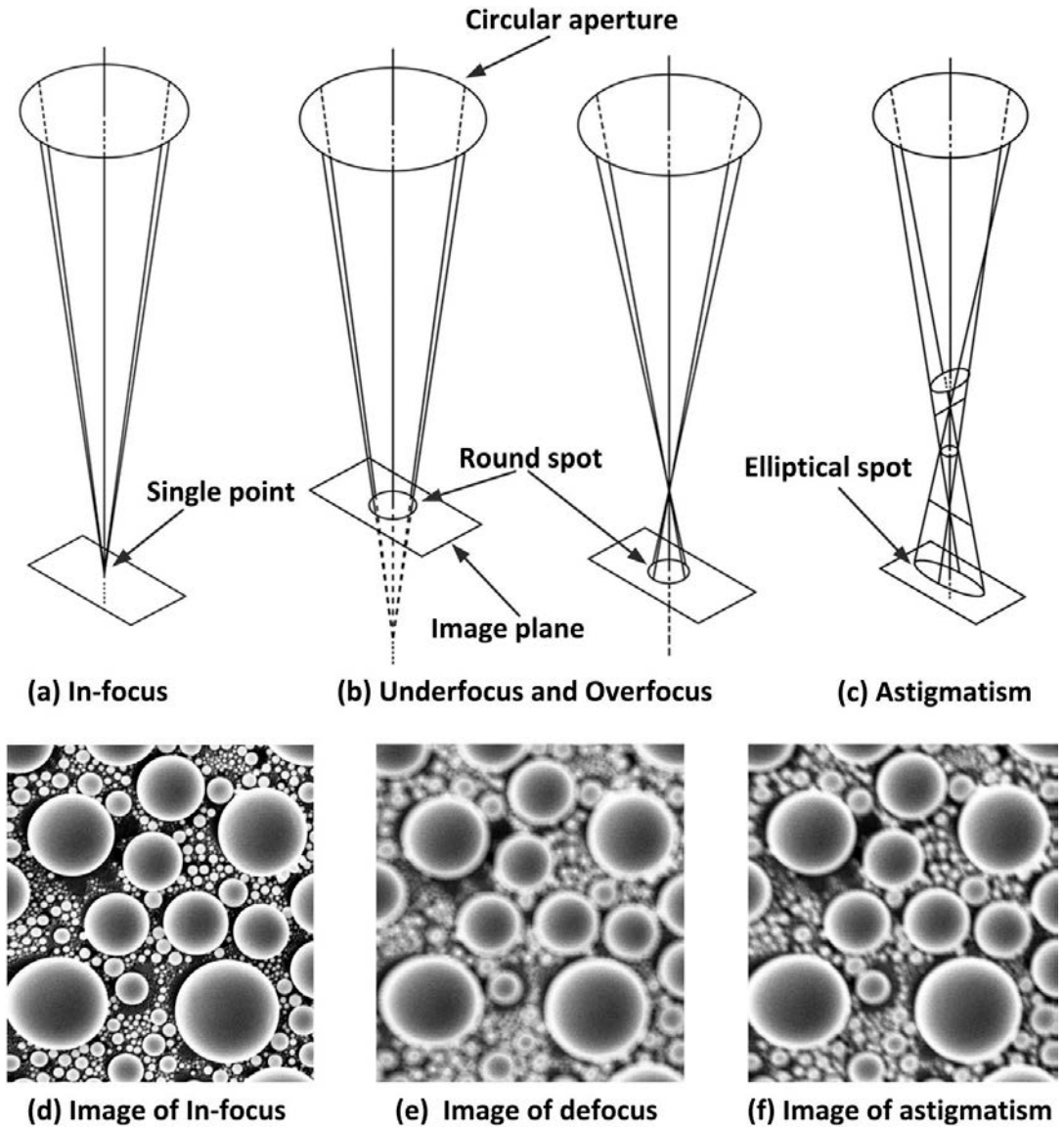

Figure from [Y. Lu, et al., A simplified focusing and astigmatism correction method for a scanning electron microscope, AIP Advances 8, 015124 (2018)]

Some quantity definitions

The phase:

$$\chi_\phi(\mathbf{g}) = \frac{1}{2p^2}\pi\lambda r^2 \Delta f_\phi(\alpha) - \frac{1}{2p^4}\pi\lambda^3 r^4 C_s + w$$

- Electron wavelength λ
- Spherical aberration C_s
- Amplitude contrast w
- Pixel size p

The bias is defined as

$$\mathrm{Bias}\left(\hat{S}_{\mathbf{y}}^{(\mathrm{p})}(\mathbf{g})\right) = \mathbb{E}\left[\hat{S}_{\mathbf{y}}^{(\mathrm{p})}(\mathbf{g})\right] - S_{\mathbf{y}}(\mathbf{g})$$

The variance is given by

$$\mathrm{Var}\left(\hat{S}_{\mathbf{y}}^{(\mathrm{p})}(\mathbf{g})\right) = \mathbb{E}\left[\left|\hat{S}_{\mathbf{y}}^{(\mathrm{p})}(\mathbf{g}) - \mathbb{E}\left[\hat{S}_{\mathbf{y}}^{(\mathrm{p})}(\mathbf{g})\right]\right|^2\right]$$

The Bartlett method

The Bartlett method is illustrated graphically on simulation to explain how a time series is converted into a power spectrum.

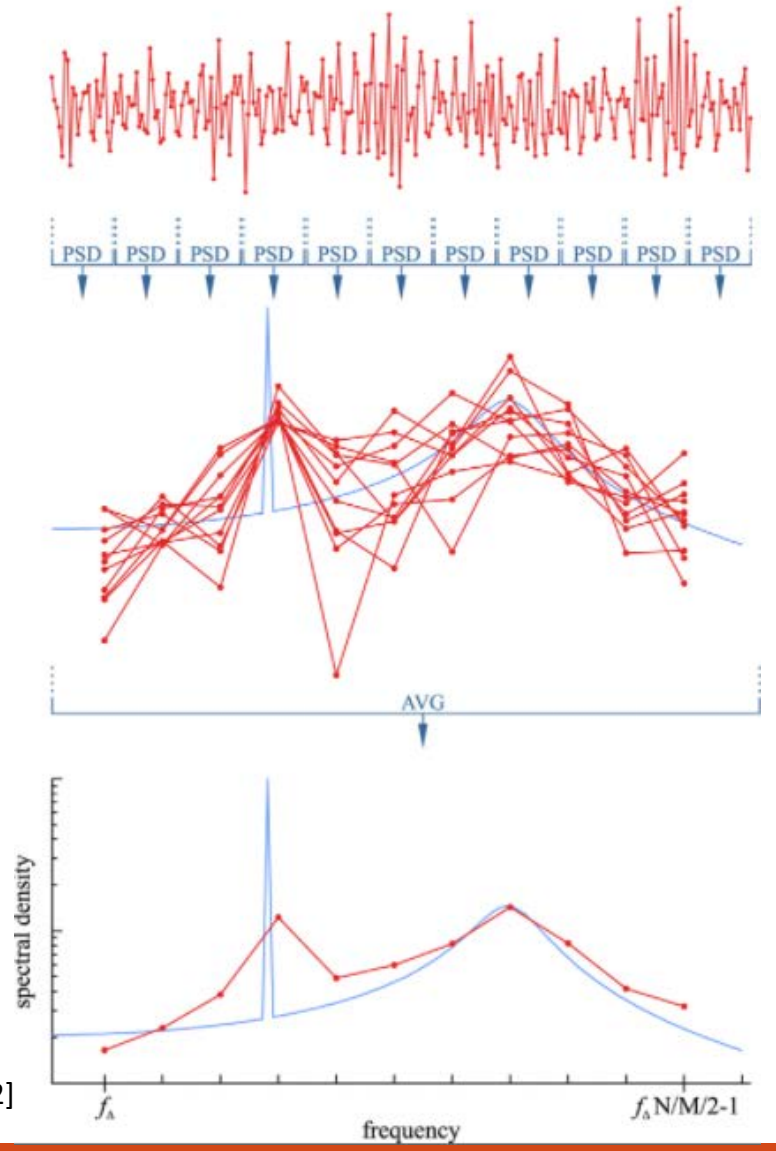

Figure is from [https://aip.scitation.org/doi/10.1063/1.4943292]

Fejér kernel

Plot of several Fejér kernels.
Plot from [https://en.wikipedia.org/wiki/Fejér_kernel]

The Fejér kernel is defined as:
$F_n(x) = \frac{1}{n}\sum_{k=0}^{n-1} D_k(x)$,
where $D_k(x) = \sum_{s=-k}^{k} e^{isx}$ is the *k*-th order Dirichlet kernel.

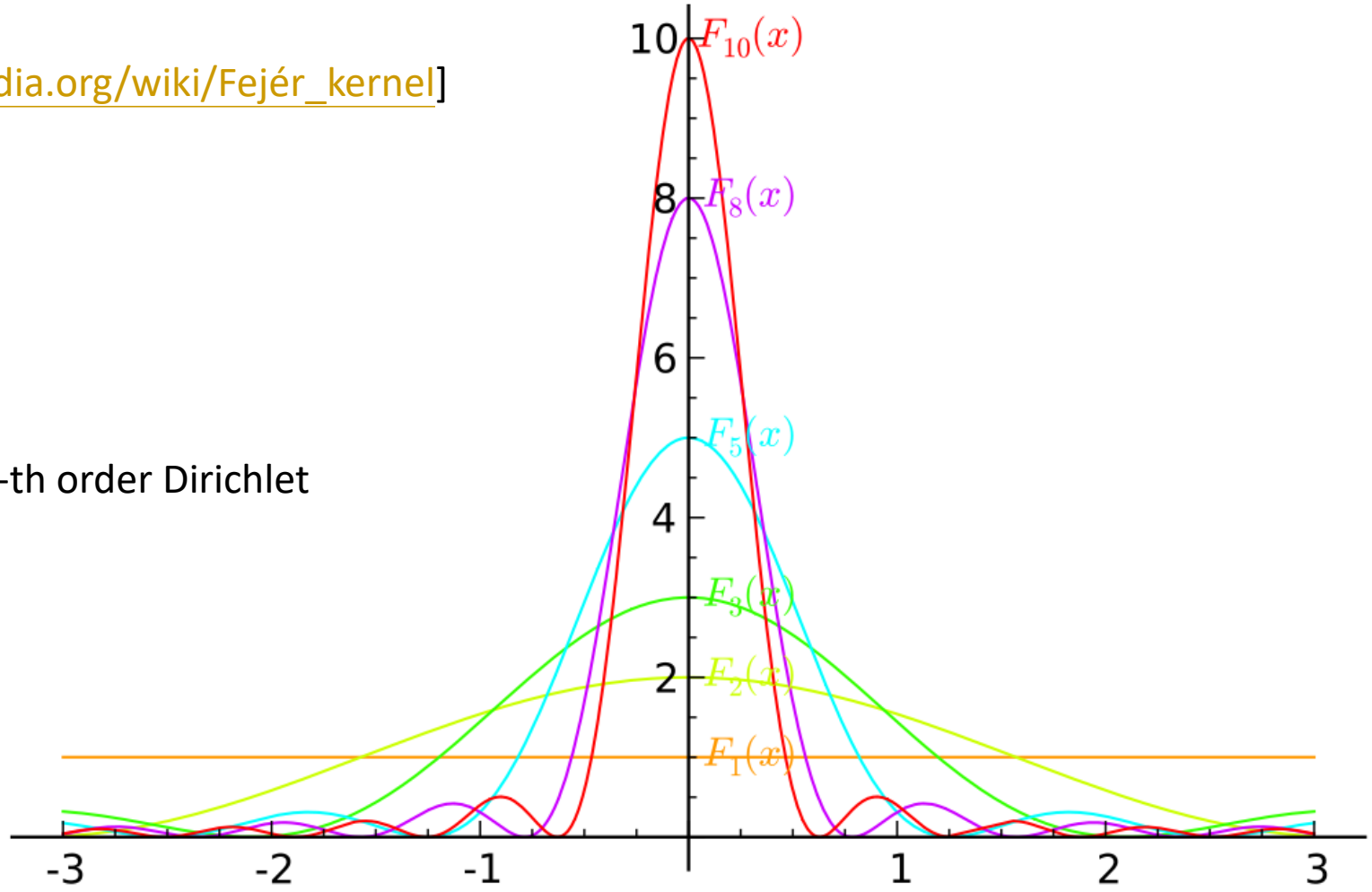

Periodogram, Welch and multitatper periodogram

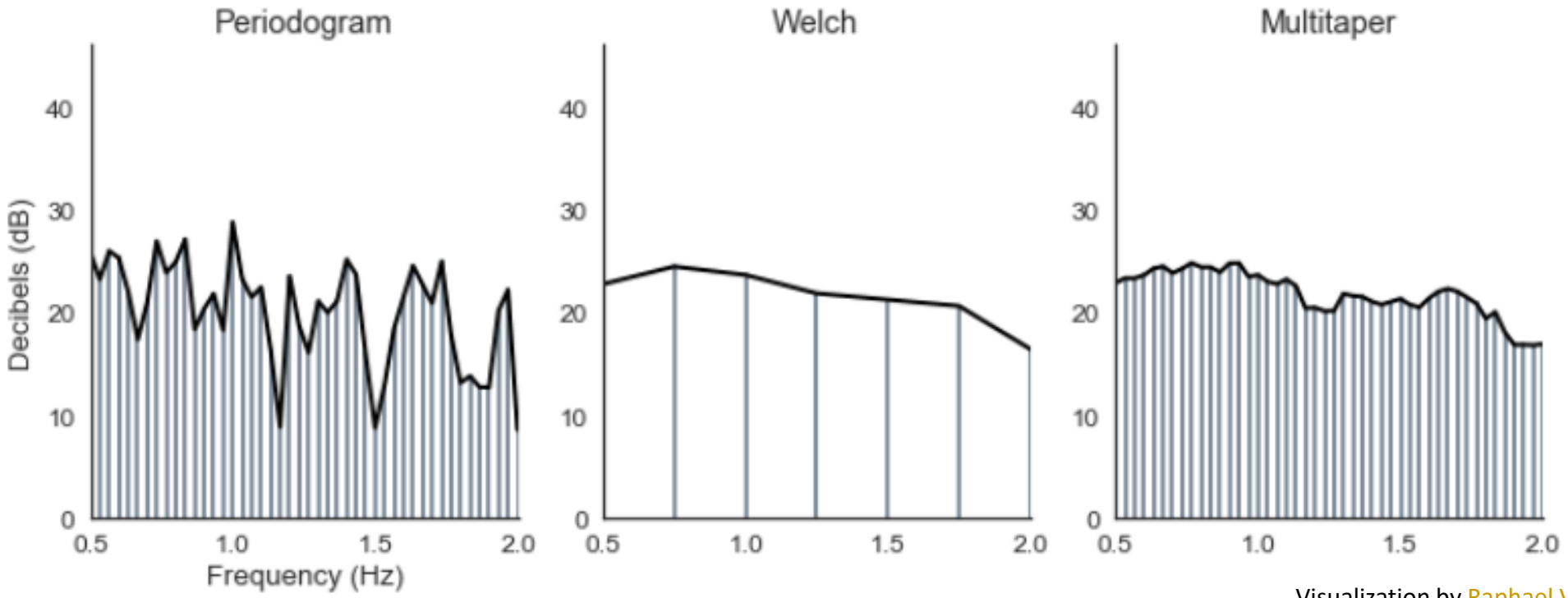

Visualization by Raphael Vallat

The classic periodogram has a good frequency resolution but has too much variance.
The Welch's periodogram has a low variance, at the cost of a lower frequency resolution.
The multitaper periodogram has high frequency resolution and low variance.

Prolate Spheroidal Wave Functions

Illustration of the first few PSWFs (real part) with bandwidth $c = 16\pi$, ordering according to their eigenvalues.

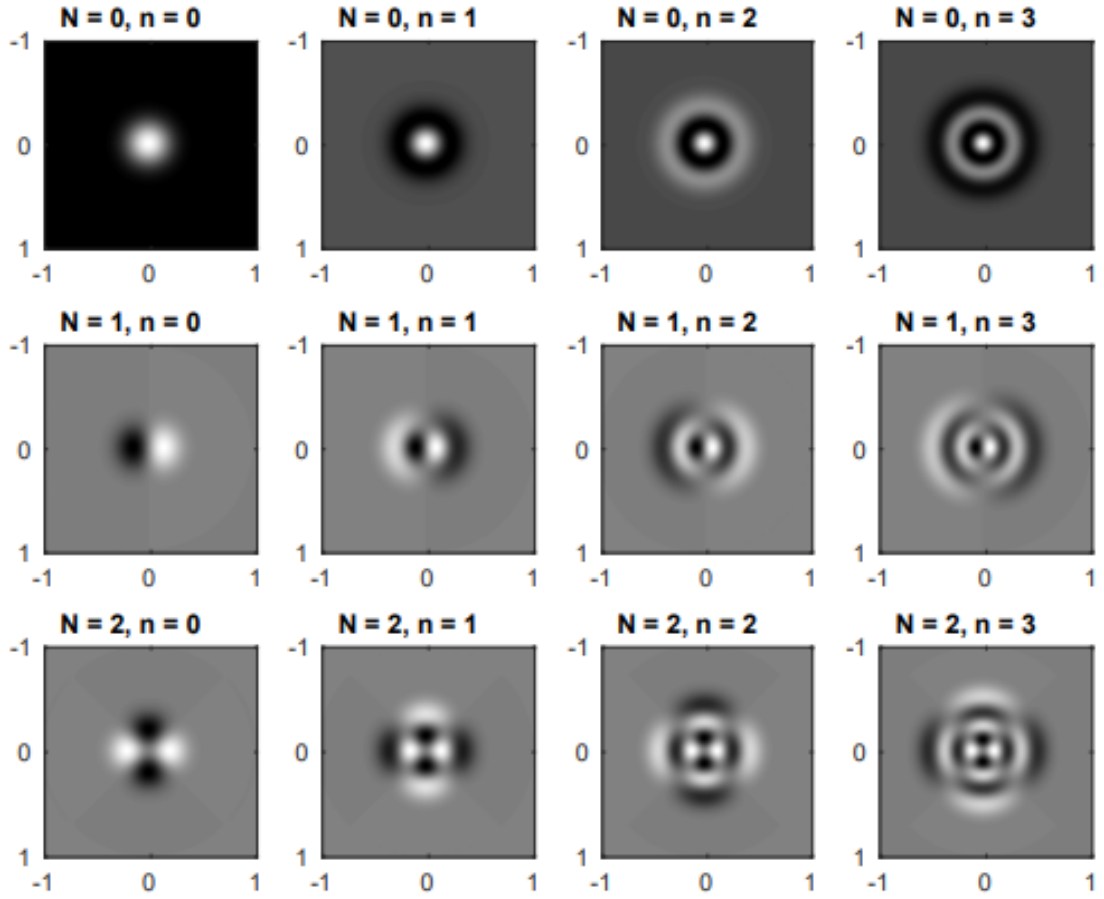

Figure from [B. Landa, et al., Steerable principal components for space-frequency localized images (2018)]

$$\text{(a) } \psi^c_{N,n}(x), x \in \mathbb{R}^2$$